Journal of Solid State Chemistry **151,** 157–162 (2000)
doi:10.1006/jssc.1999.8605, available online at http://www.idealibrary.com on IDEAL®

Structural and Magnetic Properties of Sn-, Ti-, and Mg-Substituted α-Fe_2O_3: A Study by Neutron Diffraction and Mössbauer Spectroscopy

Frank J. Berry,* Colin Greaves,† Örn Helgason,‡ Julia McManus,* Helen M. Palmer,† and Ruth T. Williams*

*Department of Chemistry, The Open University, Walton Hall, Milton Keynes MK7 6AA, United Kingdom; †School of Chemistry, The University of Birmingham, Edgbaston, Birmingham B15 2TT, United Kingdom; and ‡Science Institute, University of Iceland, Dunhagi 3, IS-107 Reykjavik, Iceland

Received May 28, 1999; in revised form October 26, 1999; accepted December 13, 1999

Hydrothermal techniques have been used to synthesize samples of α-Fe_2O_3 in which ca. 10% of the Fe cations have been replaced by Sn^{4+}, Ti^{4+}, and Mg^{2+}. Neutron powder diffraction data show the dopant ions to occupy both interstitial and substitutional sites in the corundum-related α-Fe_2O_3 structure. The details of the defect cluster depend on the charge on the dopant ion. The magnetic structures are related to that of α-Fe_2O_3 with ambient temperature Fe^{3+} moments of 4.01(5), 3.89(4), and 3.92(4) BM for Sn-, Ti-, and Mg-doped samples, respectively. The ^{57}Fe Mössbauer spectra recorded *in situ* at elevated temperatures show the Néel temperatures of Sn- and Mg-doped α-Fe_2O_3 to be between 890 and 910 K and 910 and 930 K, respectively, as compared to 950–960 K for pure α-Fe_2O_3. © 2000 Academic Press

INTRODUCTION

The doping of corundum-related α-Fe_2O_3 has attracted interest because of the magnetic, electrical, and gas sensing properties of the materials (1–9). We have recently reported on the hydrothermal synthesis and structural characterization by X-ray powder diffraction of α-Fe_2O_3 samples in which the Fe^{3+} ions had been partially replaced by Sn^{4+}, Ti^{4+}, and Mg^{2+} ions (10, 11). Interestingly, it was found that charge balance involved no change in the Fe oxidation state but was achieved by different defect clusters depending on the charge of the substituent cation (M). The defect structures can be related to the lines of octahedral Fe^{3+} ions, which are directed along [001] in the rhombohedral structure of α-Fe_2O_3. In the parent phase, pairs of face-sharing FeO_6 octahedra exist due to ordered octahedral vacancies: the chains can be represented –Fe–Fe–□–Fe–Fe–□– and are shown in Fig. 1a. For M^{4+} (M = Ti, Sn) substitutions, it was suggested (10) that clusters form which provide local charge balance: –Fe–Fe–□–M–□–M–□–M–□–Fe–Fe– chains in which three M^{4+} ions replace four Fe^{3+} ions (Fig. 1b). We shall call this a 1 : 2 : 2 cluster, since it involves one M ion on the empty octahedral (interstitial) sites in α-Fe_2O_3, two M ions substituted at Fe sites, and two vacancies introduced on to Fe sites. This contrasts with the model proposed for M^{2+} incorporation (11), in which charge balance is achieved via the formation of MMM triplets: –Fe–Fe–□–Fe–M–M–M–Fe–□–Fe–Fe– chains in which three M^{2+} ions replace two Fe^{3+} ions (Fig. 1c). This defect can therefore be represented as a 1 : 2 : 0 cluster. For both structures, the oxygen sublattice remains intact and the compositions of the substituted phases are best represented $Fe_{2-4x}M_{3x}O_3$ (M^{4+}) and $Fe_{2-2x}M_{3x}O_3$ (M^{2+}). It should be noted, however, that the sensitivity of X-ray powder diffraction data for determining complex defect structures of these types is somewhat limited. This is especially evident for Sn-doped α-Fe_2O_3, where the proposed model (involving the incorporation of both Sn and vacancies at Fe sites) results in only a small change in average scattering at the Fe sites relative to the undoped parent phase. The increased sensitivity of neutron diffraction to oxygen scattering gives it a distinct advantage over X-ray diffraction for the reliable determination of the defect structures of such oxide materials. Moreover, the technique is not subject to the problem outlined for Sn substitutions, since the scattering length of Sn (0.623×10^{-12} cm) is now less than Fe (0.954×10^{-12} cm). Also, the negative neutron scattering length for Ti (-0.344×10^{-12} cm) makes it highly unlikely that any structural inadequacy could be masked in both X-ray and neutron-diffraction experiments. We report here on the defect structures of these materials as deduced by Rietveld structure refinement of neutron powder diffraction data, and on the magnetic structures of these phases including the depression of the Néel temperature as shown by high temperature Mössbauer spectroscopy.

EXPERIMENTAL

M-substituted (M = Sn, Ti, Mg) α-Fe_2O_3 samples with nominal $M/(M + Fe)$ ratios of ca. 0.2 were prepared by

0022-4596/00 $35.00

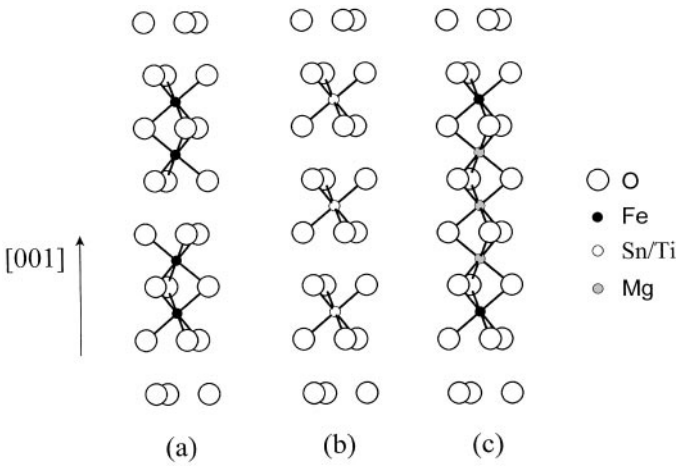

FIG. 1. (a) Linking of FeO_6 octahedra in α-Fe_2O_3. (b) Structural model involving the substitution of $4Fe^{3+}$ ions by $3M^{4+}$ ions. (c) Structural model involving the substitution of $2Fe^{3+}$ ions by $3M^{2+}$ ions.

precipitating aqueous mixtures (100 ml) of iron(III) chloride hexahydrate (24.33 g) and either tin(IV) chloride (2.08 g), titanium(IV) chloride (1.89 g), or magnesium(II) nitrate hexahydrate (2.56 g) with 0.88 aqueous ammonia (150 ml) and hydrothermally processing the suspensions (250 ml) in a Teflon-lined autoclave at 200°C and 15 atm pressure for 5 h. Owing to the nature of the synthetic process, the precise substitution level could not be reliably predicted. The products were removed by filtration and washed with 95% ethanol until no chloride ions were detected by silver nitrate solution. The products were dried under an infrared lamp. Due to the nature of the defect structures and resulting complex stoichiometries, the substituted samples will be labelled α-Fe_2O_3 [10%M].

Neutron powder diffraction data were collected at ambient temperature on the TAS3 constant wavelength ($\lambda = 1.54050$ Å) diffractometer at Risø, Denmark. Samples ($\sim$10 g) were contained in vanadium cans and data ($2\theta = 10$–$110°$, step 0.05°) were collected for approximately 6 h. The program GSAS (12) was used for refinement using scattering lengths of 0.954, 0.581, 0.623, -0.344, and 0.538 (all $\times 10^{-12}$ cm) for Fe, O, Sn, Ti, and Mg, respectively. The free ion Fe^{3+} form factor was adopted (13).

The ^{57}Fe Mössbauer spectra were recorded from powdered samples with a constant acceleration spectrometer and a ca. 400 MBq ^{57}Co/Rh source. The furnace used for the *in situ* investigations at elevated temperature has been described in detail elsewhere (14). The sample thickness was 50–80 mg cm^{-2}. The linewidth (FWHM) of the calibration spectrum was 0.24 mms^{-1}. The chemical isomer shift data are quoted relative to the centroid of the metallic iron spectrum at room temperature.

RESULTS AND DISCUSSION

α-Fe_2O_3 [10% Sn] and α-Fe_2O_3 [10% Ti]

The neutron powder diffraction patterns recorded from α-Fe_2O_3 [10% Sn] and α-Fe_2O_3 [10% Ti] were best refined according to the model previously used (10) to refine the X-ray powder diffraction data from samples with similar compositions. The patterns showed no evidence of impurity phases. The analysis of the data showed the dopant ions to occupy two distinct sites in the corundum-related structure of α-Fe_2O_3 in which the Fe^{3+} ions are distributed in an ordered fashion over 2/3 of the octahedral sites within a framework of hexagonally close-packed O^{2-} ions (Fig. 1a). Refinements in which the oxygen occupation number was varied confirmed that the oxygen sublattice was complete, and it was clear that the structures involved both interstitial and substitutional M cations (Fig. 1b). The presence of M in the interstitial sites would produce strong cation–cation repulsions from the two adjacent face-shared FeO_6 octahedra. Elimination of the cations from these two sites results in two additional octahedral sites (respectively, above and below the cations removed), which do not involve face-sharing and which are therefore attractive for occupation by additional M ions. In this way, the structural model shown in Fig. 1b, involving the 1:2:2 clusters, was confirmed. In the final refinements, the cation site occupancies were constrained in accordance with the model.

The complete set of final refined parameters are shown in Table 1, and conventional observed and calculated profiles are shown in Figs. 2a and 2b. The refined cation occupancies, with the constraint of the defect model, yields values for M:Fe of 13.4(1.3)% and 13.4(0.9)% for M = Sn and Ti, respectively, indicative of $M/(M + \text{Fe})$ of 0.24 and sample formulas of $Fe_{1.698}M_{0.228}O_3$. The structural parameters show little deviation from those of ideal α-Fe_2O_3, which suggests that the defect clusters can be incorporated with very little lattice strain. The unit cell volumes of α-Fe_2O_3, α-Fe_2O_3 [10% Sn], and α-Fe_2O_3 [10% Ti] are 301.9(1) Å^3 (15), 302.15(7) Å^3, and 301.52(4) Å^3, respectively. Although very small, the changes in unit cell size are consistent with the ionic radii for six-coordinate Fe^{3+}, Sn^{4+}, and Ti^{4+} (0.65, 0.69, and 0.61 Å, respectively (16)).

The magnetic structures for both samples were found to be very similar to that of undoped α-Fe_2O_3 above the Morin transition—antiferromagnetic with layers of Fe^{3+} having moments perpendicular to [001] and aligned antiparallel to the moments in adjacent layers. The moments for the Fe^{3+} ions in α-Fe_2O_3[10% Sn] and α-Fe_2O_3[10% Ti] were found to be 4.01(5) and 3.89(4) BM, respectively. These values are less than the 5 BM expected for Fe^{3+} the reduction being primarily due to thermal effects. The moments are typical for antiferromagnetic Fe^{3+}-containing oxides at temperatures which are substantially below their Néel temperatures. The impact of the dopant ions on the Néel

TABLE 1
Refined Structural Parameters for α-Fe_2O_3[10% Sn], α-Fe_2O_3[10% Ti], and α-Fe_2O_3[10% Mg]

α-Fe_2O_3[10% Sn]

Atom	x/a	y/b	z/c	$U_{iso} \times 100/Å^2$	Site occupancy
O	0.3079(6)	0	$\frac{1}{4}$	0.73(11)	1
Fe	0	0	0.3547(2)	0.63(7)	0.849(12)[a]
Sn1	0	0	0.3547(2)	0.63(7)	0.076(6)[a]
Sn2	0	0	0	0.63(7)	0.076(6)[a]

R-3*c*: $a = 5.0369(4)$, $c = 13.752(1)$ Å
Fe^{3+} magnetic moment 4.01(5) BM
$R_{wp} = 8.7\%$, $R_p = 6.8\%$, $R_{exp} = 5.9\%$

α-Fe_2O_3[10% Ti]

Atom	x/a	y/b	z/c	$U_{iso} \times 100/Å^2$	Site occupancy
O	0.3083(5)	0	$\frac{1}{4}$	0.85(9)	1
Fe	0	0	0.3546(1)	0.52(6)	0.848(7)[a]
Ti1	0	0	0.3546(1)	0.52(6)	0.076(4)[a]
Ti2	0	0	0	0.52(6)	0.076(4)[a]

R-3*c*: $a = 5.0293(2)$, $c = 13.7648(9)$ Å
Fe^{3+} magnetic moment 3.89(4) BM
$R_{wp} = 7.7\%$, $R_p = 5.9\%$, $R_{exp} = 5.1\%$

α-Fe_2O_3[10% Mg]

Atom	x/a	y/b	z/c	$U_{iso} \times 100/Å^2$	Site occupancy
O	0.3072(5)	0	$\frac{1}{4}$	0.40(8)	1
Fe	0	0	0.3547(1)	0.63(5)	0.943(8)[b]
Mg1	0	0	0.3547(1)	0.63(5)	0.057(8)[b]
Mg2	0	0	0	0.63(5)	0.057(8)[b]

R-3*c*: $a = 5.0506(2)$, $c = 13.7919(9)$ Å
Fe^{3+} magnetic moment 3.92(4) BM
$R_{wp} = 8.4\%$, $R_p = 6.5\%$, $R_{exp} = 5.5\%$

[a]Site occupancies Fe = 1 − 2M1; M1 = M2; M = Sn, Ti
[b]Site occupancies Fe = 1 − Mg1; Mg1 = Mg2

temperature was examined by ^{57}Fe Mössbauer spectroscopy. The ^{57}Fe Mössbauer spectra recorded at 298 K from α-Fe_2O_3 and the Sn- and Ti-doped variants (Fig. 3, Table 2) showed the doped materials to be best fitted to two sextet patterns with chemical isomer shifts and quadruple splittings similar to that for α-Fe_2O_3. One component (H = ca. 50 T) of narrow linewidth accounted for ca. 75% of the spectral area whilst the other broader line component (H = ca. 48 T) constituted the remainder of the spectrum and resisted resolution into a specific hyperfine magnetic field distribution. The component with a larger hyperfine magnetic field can be associated with the Fe^{3+} ions without Sn^{4+}/Ti^{4+} ions in nearby lattice sites whereas the component with lower hyperfine magnetic field reflects the lower spin density at Fe^{3+} in the vicinity of Sn^{4+}/Ti^{4+} nearest cation neighbors.

A series of ^{57}Fe Mössbauer spectra recorded *in situ* at temperatures between 300 and 900 K for α-Fe_2O_3[10% Sn]

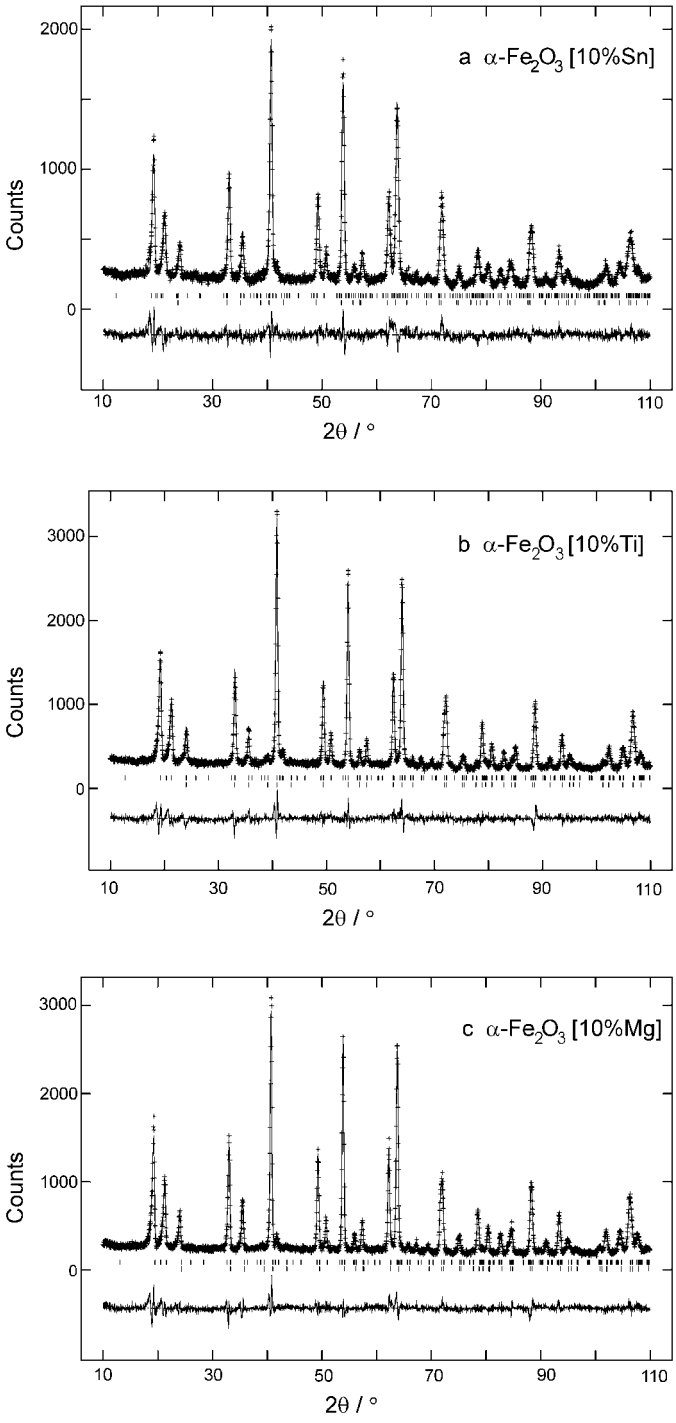

FIG. 2. Observed, calculated, and difference neutron powder diffraction patterns recorded from (a) α-Fe_2O_3[10% Sn], (b) α-Fe_2O_3[10% Ti], and (c) α-Fe_2O_3[10% Mg]. In each case, the upper and lower vertical tick marks show the positions of nuclear and magnetic reflections.

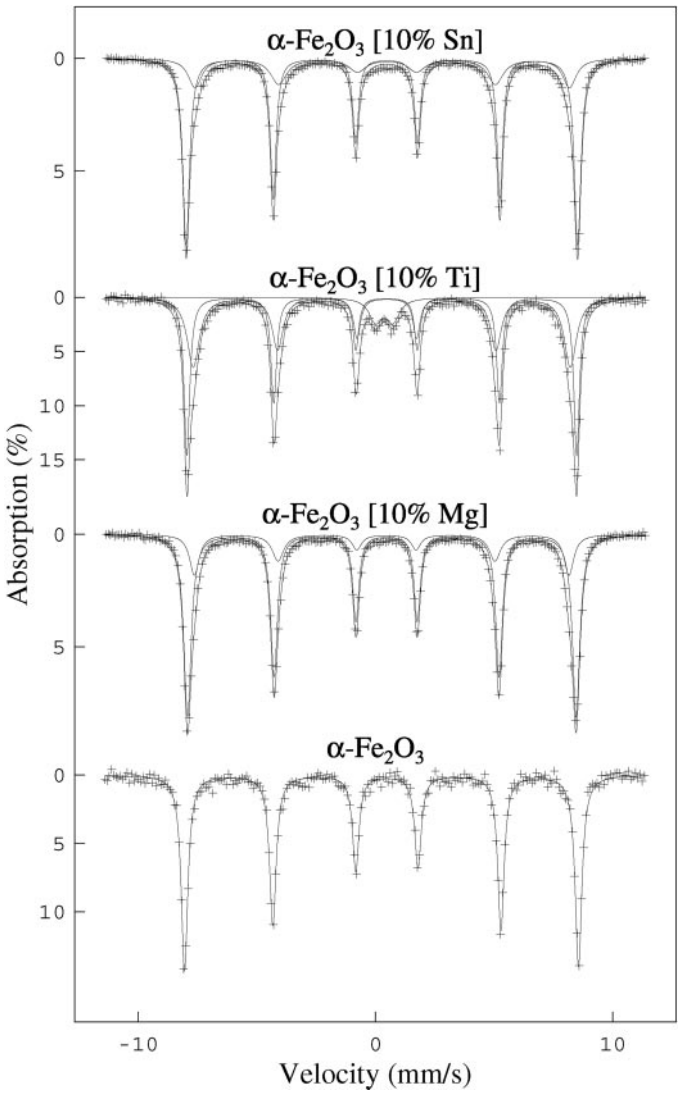

FIG. 3. ^{57}Fe Mössbauer spectra recorded at 298 K from α-Fe_2O_3 and α-Fe_2O_3[10% Sn], α-Fe_2O_3[10% Ti], and α-Fe_2O_3[10% Mg]

are shown in Fig. 4. The hyperfine magnetic fields characterizing the two sextet patterns decrease in value as the temperature increases. The appearance of a doublet at 500–600 K is indicative of some of the particles being sufficiently small to show paramagnetic behavior. The growth of the doublet with increasing temperature is consistent with the progressive development of the paramagnetic phase. The results recorded from α-Fe_2O_3[10% Sn] (Fig. 4) show that tin-doped α-Fe_2O_3 is almost completely paramagnetic at 900 K. The variation of the spectral component with the larger hyperfine magnetic field with temperature is shown in Fig. 5. Extrapolation of the data recorded between 800 and 870 K enables a Néel temperature between 890 and 910 K to be determined. It should be noted that the ^{57}Fe Mössbauer spectra gave no evidence for the presence of Fe^{2+} as

TABLE 2
^{57}Fe Mössbauer Parameters Recorded at 298 K from α-Fe_2O_3[10% Sn], α-Fe_2O_3[10% Ti], and α-Fe_2O_3[10% Mg]

Compound	$\delta \pm 0.01$ (mms^{-1})	$\Delta \pm 0.01$ (mms^{-1})	$H \pm 1$ (T)	$\Gamma \pm 0.02$ (mms^{-1})	Spectral area ± 5 (%)
α-Fe_2O_3	0.36	−0.11	51.4	0.31	100
α-Fe_2O_3[10% Sn]	0.38	−0.11	51.0	0.31	70
	0.36	−0.10	49.0	0.30–0.80	30
α-Fe_2O_3[10% Ti]	0.37	−0.10	50.8	0.29	62
	0.38	−0.11	49.0	0.30–0.60	30
	0.37	0.72		0.67	8
α-Fe_2O_3[10% Mg]	0.38	−0.10	50.0	0.31	75
	0.38	−0.10	48.0	0.30–0.70	25

a result of doping with Sn^{4+} and are therefore consistent with the achievement of charge balance without reduction of Fe^{3+} to Fe^{2+} (see above).

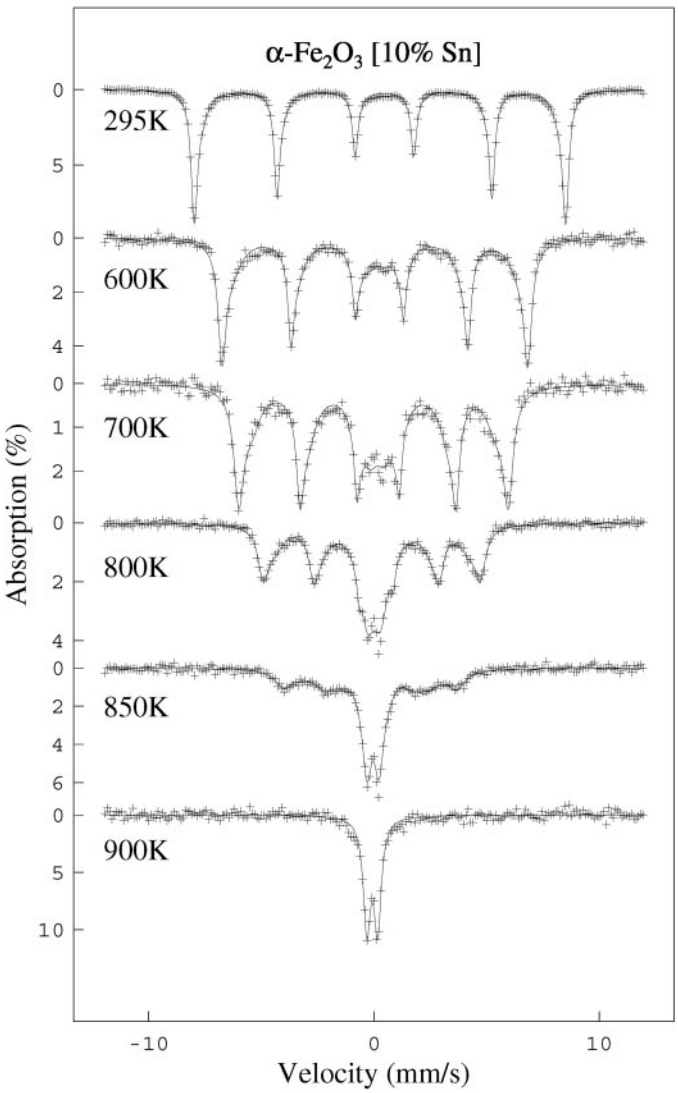

FIG. 4. ^{57}Fe Mössbauer spectra recorded *in situ* from α-Fe_2O_3 [10% Sn] as a function of increasing temperature.

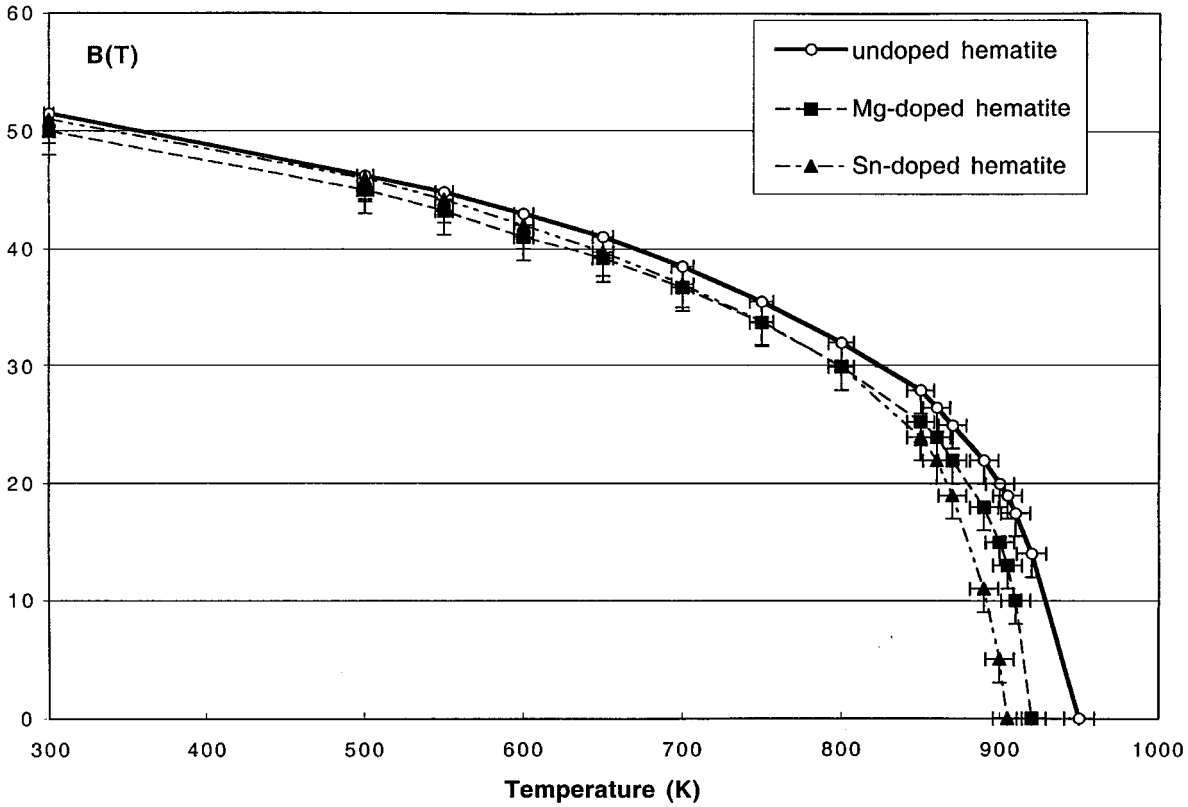

FIG. 5. Variation of hyperfine magnetic field for the component with high hyperfine magnetic field as a function of increasing temperature for α-Fe_2O_3, α-Fe_2O_3[10% Sn], and α-Fe_2O_3[10% Mg].

α-Fe_2O_3[*10% Mg*]

The neutron powder diffraction data showed no evidence of impurity phases and confirmed the structure previously (11) deduced from X-ray powder diffraction and interpreted in terms of the Mg^{2+} ions occupying both substitutional and interstitial sites. All refinements in which the O occupancy was allowed to vary implied no vacancies on the oxygen sublattice and provided strong evidence that a simple model involving Mg substitution and oxygen vacancies was invalid. The defect 1:2:0 cluster (Fig. 1c) is different from that in the materials containing Sn^{4+} and Ti^{4+} in that the lower charge on magnesium allows the formation of a linear cluster of three Mg^{2+} species. Cation site occupancies, constrained according to this model, provided a good fit to the data as shown in Fig. 2c. The magnetic structure is similar to that exhibited by the Sn- and Ti-doped materials with a magnetic moment on Fe^{3+} of 3.92(4) BM. The refined structural parameters are summarised in Table 1. The Mg:Fe ratio of 9.1(1.3)% is in reasonable agreement with the Mg:Fe ratio used in the synthesis procedure, 11.1%, and is consistent with Mg/(Mg + Fe) = 0.17 and a formulation $Fe_{1.886}Mg_{0.171}O_3$. The unit cell volume for α-Fe_2O_3[10% Mg], 304.68(4) Å^3, is significantly larger than that for α-Fe_2O_3, which reflects the larger radius of Mg^{2+} (0.72 Å) (16), but may also in part relate to the increased cation repulsions associated with the interstitial Mg^{2+} ions. In contrast to the 1:2:2 clusters proposed for M^{4+} incorporation, the interstitial ions in the 1:2:0 clusters are not adjacent to vacancies on the Fe sublattice.

The ^{57}Fe Mössbauer spectrum recorded at 298 K from α-Fe_2O_3[10% Mg] was also best fitted to two sextet components (Fig. 3) with hyperfine magnetic fields which decrease in value as the temperature increases (Fig. 6). The progressive development of a doublet characteristic of paramagnetic Fe^{3+} in spectra recorded *in situ* at increasing temperatures shows the material to be almost completely paramagnetic at 900 K. The variation in magnitude of hyperfine magnetic field with increasing temperature (Fig. 5) enables a Néel temperature between 910 and 930 K to be determined. The ^{57}Fe Mössbauer spectra showed no evidence for the oxidation of Fe^{3+} to Fe^{4+} as a result of the incorporation of Mg^{2+} in α-Fe_2O_3 and are therefore consistent with charge balance not involving a change in the oxidation state of iron (see above).

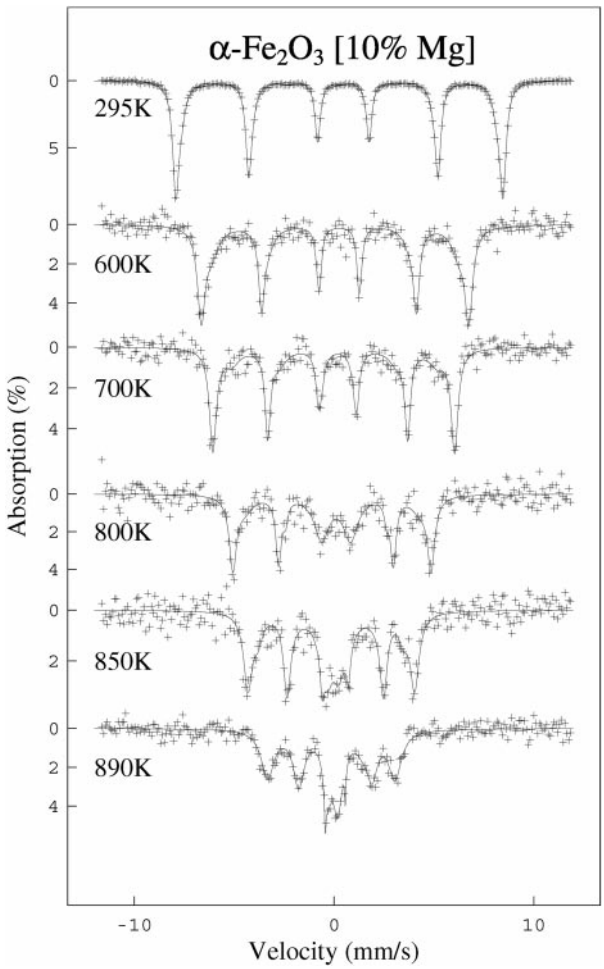

FIG. 6. ^{57}Fe Mössbauer spectra recorded *in situ* from α-Fe_2O_3 [10% Mg] as a function of increasing temperature.

ACKNOWLEDGMENTS

We thank the EPSRC for the award of studentships (J.M. and H.M.P.), and B. Lebech for experimental assistance with the collection of neutron diffraction data.

REFERENCES

1. F. J. Morin, *Phys. Rev.* **83,** 1005 (1951).
2. N. Uekawa, M. Watanabe, K. Kaneko, and F. Mizukami, *J. Chem. Soc. Faraday Trans.* **91,** 2161 (1995).
3. P. B. Fabritchnyi, E. V. Lamykin, A. M. Babechkin, and A. N. Nesmeianov, *Solid State Commun.* **11,** 343 (1972).
4. F. Schneider, K. Melzer, H. Mehner, and G. Deke, *Phys. Status Solidi A* **39,** K115 (1977).
5. M. Takano, Y. Bando, N. Nakanishi, M. Sakai, and H. Okina, *J. Solid State Chem.* **68,** 153 (1987).
6. S. Music, P. Popovic, M. Metikos-Hukovicc, and G. Gvozdic, *J. Mater. Sci. Lett.* **10,** 197 (1991).
7. H. Kanai, H. Mizutani, T. Tanaka, T. Funabiki, S. Yoshida, and M. Takano, *J. Mater. Chem.* **2,** 703 (1992).
8. P. Bonzi, C. E. Pepero, F. Parmigiani, C. Perego, G. Sberveglieri, and G. Quattroni, *J. Mater. Res.* **9,** 1250 (1994).
9. Y. Lin, W. Zhu, M. S. Tse, and S. Y. Shen, *J. Mater. Sci. Lett.* **14,** 1185 (1995).
10. F. J. Berry, C. Greaves, J. G. MacManus, M. Mortimer, and G. Oates, *J. Solid State Chem.* **130,** 272 (1997).
11. F. J. Berry, A. Bohorquez, C. Greaves, J. G. McManus, E. A. Moore, and M. Mortimer, *J. Solid State Chem.* **140,** 428 (1998).
12. A. C. Larson and R. B. Von Dreele, "General Structure Analysis System," University of California, 1985–1990.
13. R. E. Watson and A. T. Freeman, *Acta Crystallogr.* **14,** 27 (1961).
14. Ö. Helgason, M. P. Gunnlaugsson, K. Jónsson, and S. Steinhorsson, *Hyperfine Interact.* **91,** 595 (1994).
15. L. W. Finger and R. M. Hazen, *J. Appl. Phys.* **51,** 5362 (1980).
16. R. D. Shannon, *Acta Crystallogr. A* **32,** 751 (1076).